In-orbit calibration activities of the XMM-Newton EPIC Cameras

D.H. Lumb[a], Ph. Gondoin[a], M.J.L. Turner[b], A.F. Abbey[b], P.J. Bennie[b], S. Sembay[b], G. Griffiths[b], P. Ferrando[c], J-L. Sauvageot[c], E.Belsole[c], C.Pigot[c], U.G. Briel[d], K. Dennerl[d], F. Haberl[d], G. Hartner[d], E. Kendziorra[f], M. Kirsch[f], M. Kuster[f], S. Molendi[g], G. Villa[g], A. Tiengo[g,e], A. Lagostina[g,e], N La Palombara[g] E. Serpell[e]

[a] European Space Research and Technology Center, 2200 AG Noordwijk zh, the Netherlands

[b] X-Ray Astronomy Group, University of Leicester, Leicester LE1 7RH, U.K.

[c] Commissariat a l'Energie Atomique, 91191 Gif-sur-Yvette cedex, France

[d] Max-Planck-Institut fur Extraterrestrische Physik, 85748 Garching, Germany

[e] XMM-Newton Science Operations Centre, Villafranca Satellite Tracking Station, 28080 Madrid, Spain

[f] Institut fur Ast. & Astrophysik, University Tubingen, D72076 Tubingen, Germany

[g] IFCTR del CNR, via Bassini 15, 20133 Milano, Italy

ABSTRACT

The combined effective area of the three EPIC cameras of the XMM-Newton Observatory, offers the greatest collecting power ever deployed in an X-ray imaging system. The resulting potential for high sensitivity, broad-band spectroscopic investigations demands an accurate calibration. This work summarises the initial in-orbit calibration activities that address these requirements. We highlight the first steps towards effective area determination, which includes the maintenance of gain and CTI calibration to allow accurate energy determination.We discuss observations concerning the timing and count-rate capabilities of the detectors. Finally we note some performance implications of the optical blocking filters.

Keywords: XMM−Newton, x-ray astronomy, CCDs, calibration

1. INTRODUCTION

On December 10 1999 the XMM-Newton space observatory was placed in a 48 hours period orbit by the first commercial Ariane V launcher. The High Throughput X-ray Spectroscopy Mission XMM-Newton[1] is a "Cornerstone" project in the ESA long-term programme for space science. Its primary objective is to perform high throughput spectroscopy of cosmic x-ray sources over a broad band of energies ranging from 0.1 keV to 10 keV down to a limiting flux of 10^{-15} ergs s^{-1} cm^{-2}. The XMM-Newton payload includes:

- Three grazing incidence telescopes[2] which provide an effective area higher than 4000 cm^2 at 2 keV and 1600 cm^2 at 8 keV and an image quality better than 15 arcsec Half Energy Width (HEW),
- Three CCD imaging cameras (EPIC)[3,4], one at the prime focus of each telescope, which provide imaging in a 30 arcmin field of view and broadband spectroscopy with a resolving power of between 5 and 60 in the energy band 0.1 to 15 keV,
- Two reflection grating spectrometers (RGS)[5] which provide spectroscopy between 0.2 and 2 keV with a resolving power of over 250 at 0.5 keV,
- A Uv/optical monitor (OM)[6] which permits simultaneous monitoring of x-ray sources in the UV and optical range included between 160 and 600nm.

The EPIC (European Photon Imaging Camera) consortium is a pan-European collaboration of Universities and research facilities from the U.K., France, Germany and Italy. Behind two mirror systems equipped with Reflection Grating Arrays are mounted the EPIC MOS cameras, and behind the unobscured mirror system an EPIC PN camera. The details of these two detector systems are provided in references 3 and 4. The first in-flight images and performance highlights were presented in Turner et al[7], and Briel et al[8]. Briefly, the MOS cameras each comprise 7 conventional CCDs, closely butted to form a ∼65mm (30 arcminutes) diameter field of view. The CCDs are nonetheless specially optimised to enhance the low- and high-energy X-ray responses. They offer 1 arcsecond pixel sizes, a normal readout time resolution of 2.6 seconds and energy resolution at 1keV of 70eV FWHM. The PN camera is comprised of a wafer scale monolithic array of 12 CCDs, 60 mm square. The pixel size of 150μm subtends 4 arcsec on the sky. A fast multi-parallel readout allows 73 ms frame times in normal full-field coverage. The energy resolution is comparable with the MOS camera, while its combination of thick detection layer and thin dead layer provides excellent efficiency over the whole XMM energy band.

The spatial domain performance of EPIC is intimately related to that of the XMM-Newton mirrors, and the accompanying paper[9] should be consulted for such aspects. This paper concentrates on the spectroscopic performance. Table 1 summarises some of the more important celestial observations made during the initial in-flight calibration programme for EPIC.

Target Name	Revolution	Goal
NGC2516	58,60 & 92	Determine boresight and CCD alignments
LMC X-3	66 & 92	PSF at different count rates
G21.5-09	60,61, 62	Effective area and Vignetting
A496	48	Vignetting
PKS0537-28	51	Effective Area
MS0737+7441	63	Effective area
MS1229+6430	82	Effective area
Mkn205	75	Effective area
PKS0312-770	57	On axis PSF of MOS in low pile-up flux rate, comparison with CHANDRA.
1ES0102-72	65	Low energy emission line gain and
and N132D	76 & 83	provide cross check with CHANDRA
Crab Nebula	54 & 56	On-axis effective area in diffuse source. Off-axis stray light measurements in X-ray baffle performance
CAL 83	68	Filter X-ray transmission (O band)
HZ43	89	Filter X-ray transmission (C band)
Alpha Pic	79	Optical filter transmission
EXO0748-676	50	Mode Timing calibration
PSR0540-693	85	Mode Timing calibration

Table 1. Summary of key celestial calibration targets for EPIC

2. CTI AND GAIN

Before launch there was a concern that the proton damage experienced by the CHANDRA ACIS front-illuminated CCDs[10] could affect in a similar way the EPIC MOS cameras (the two satellites are in comparable, highly eccentric orbits, and the CCD technologies are very similar). The effects are reduced in EPIC by using a closed filter position, whereby 1mm of aluminium shielding can be placed in the path of soft protons scattered from the mirrors. This filter mechanism was designed with high reliability, to be employed at every perigee passage. Following the CHANDRA experience it was also decided to close the filter when the on-board radiation monitor detected particle flares. This practice, using conservative monitor thresholds, would prevent any significant degradation of the charge transfer efficiency. The major damage could then result from the total dose of high energy protons from major solar flares or encountered at perigee belt passage.

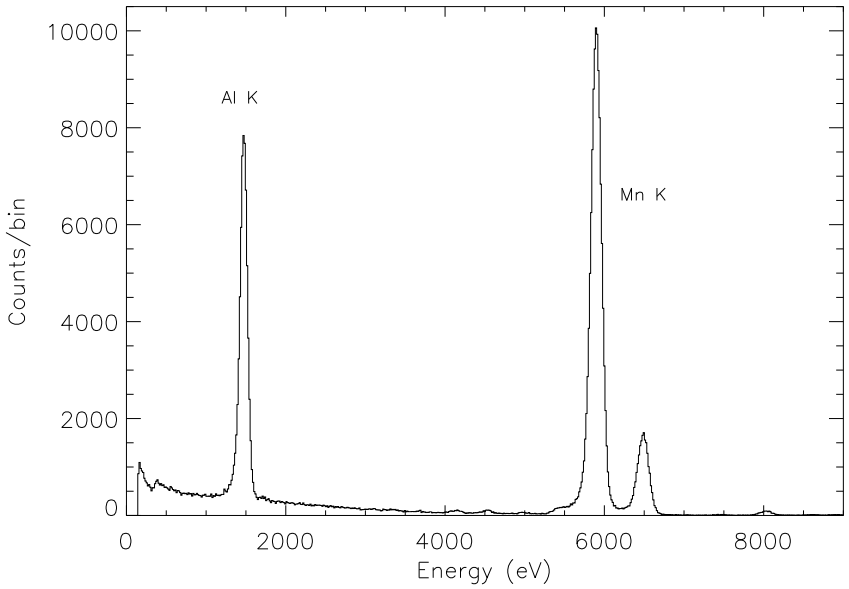

Figure 1. Internal calibration source spectrum, as observed with EPIC PN

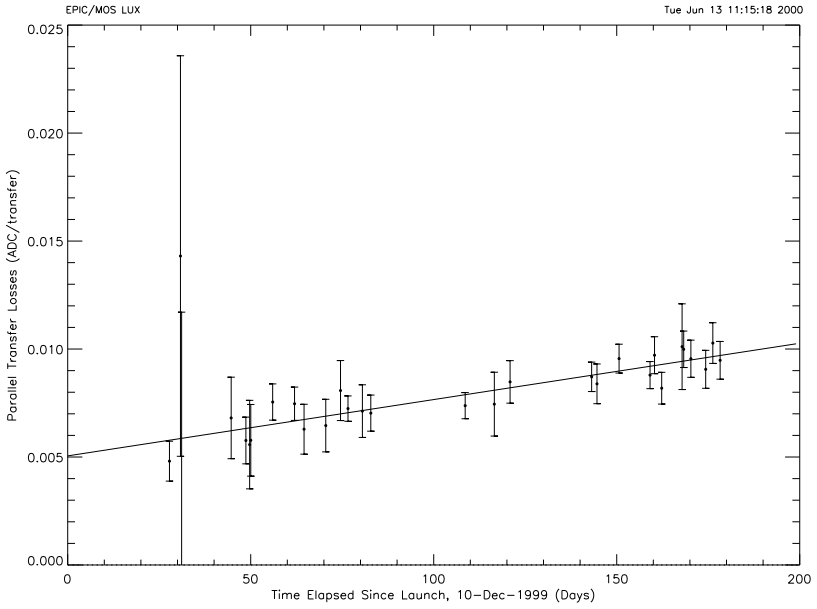

Figure 2. Evaluation of EPIC MOS CTI with time. Mn Kα emision line ($\sim$1790ADU peak position)

To monitor the charge transfer loss as a function of pixel position, an internal calibration source is deployed regularly. This source comprises a primary Fe^{55} source, with secondary Al K fluorescence, which illuminates quasi-uniformly the whole CCD array (Figure 1). By measuring the centroid of the detected emission line energies as a function of position, the charge loss per pixel transfer can be calculated.

Figure 2 shows the measurement of CTI as a function of time. Close examination shows that an on-axis source located at pixel (300,300) in the MOS camera would have experienced a *change* in charge loss of ∼1 ADU since launch. On a signal of 1790ADU for the calibration source, this is less than 0.1% of the mean value. Extrapolating for an extended mission lifetime of 10 years, we therefore predict that loss of energy resolution will not affect scientific goals, providing that the CTI is monitored continually and corrected appropriately. Potential damage (e.g. due to major solar flares) could be accommodated in the MOS cameras by a change in operation temperature to ∼20 degrees colder than currently used. For the PN cameras we see no measureable degradation since launch.

The internal calibration source is also used to measure the gain of the cameras, i.e. the energy to Analogue-Digital conversion units. Celestial measurements using supernova remnants with bright emission lines have in addition been used, because the slight non-linearities in the gain function are not well-sampled by the 3 bright emission line energies of the calibration source. The analysis of these data is more complex, as a result of both the uncertainties in the parameters of the astrophysical plasma models, and the intimate connection between gain and the energy redistribution response functions for spectral fitting. Figure 3 shows some typical results from spectral fitting obtained during the verification of the gain with celestial targets. We note there are minor inconsistencies still to be resolved, but in general energies are calibrated to a few eV.

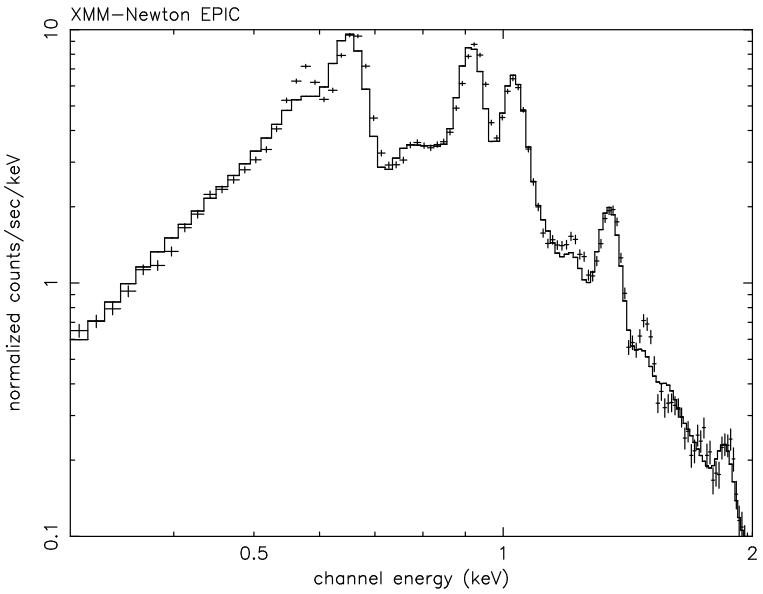

Figure 3. Spectral fitting and energy resolution in EPIC MOS - 1ES0102-72 supernova remnant data (crosses), thermal spectrum+power law model(histogram)

The correctness of the energy calibration is also indicated by observations of the iron line energy in cluster A496. Figure 4 displays the spectrum of this source measured with the PN camera. The centroid of the iron line feature matches exactly that which would be predicted for the known red-shift of the cluster.

3. EFFECTIVE AREA

First measurements of the effective area confirm the predictions pre-launch (see accompanying papers[8,12,13]). With an effective area larger than previously deployed, any systematic effects of incorrectly modelled effective area become larger than statistical variations for fainter fluxes, or for shorter observations than heretofore. Determining the effective area and spectral response distributions are thus the most important goals for XMM-Newton calibration.

The flight model detector of the PN camera was replaced with the Flight Spare, rather late in the hardware programme. As a result the ground calibration of energy response was not as detailed as originally planned. Using the limited set of ground calibration data, and the in-flight calibration sources, a response model for this flight spare detector has been developed. Fortunately the quantum efficiency of the PN CCDs is uniformly high, well-modelled

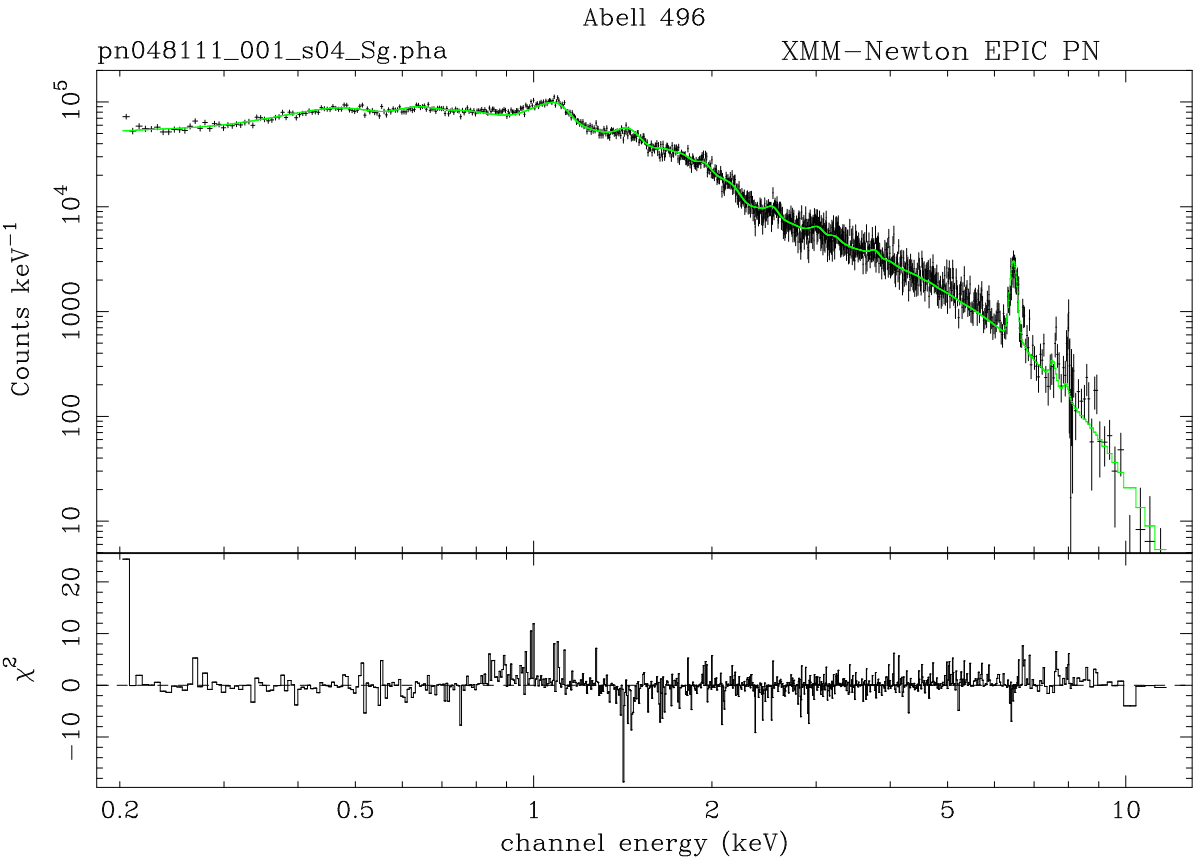

Figure 4. Spectral fitting of the EPIC PN observation A496. Note the redshifted iron line feature at ∼6keV. The large effective area of the EPIC PN allows measurements to ≥10keV, and hence enables much improved measurements of hot plasmas and leverage on measuring power law slopes.*Data courtesy of XMM-Newton Guaranteed Time Observations of J Bleeker, SRON, Netherlands*

and confirmed in a number of flight-like detectors in white-light synchrotron beams. Likewise, for the MOS CCDs, some individual CCD chips were replaced after the nominal calibration programme, in order to furnish the flight cameras with a complement of high performance devices. The spectral response distributions of the MOS cameras were extensively calibrated with monochromatised radiation at a synchrotron facility. However the quantum efficiency could not be accurately measured at some energies. The efficiency itself proved complex to model, due to the many different surface and electrode features of the CCD design.

To verify these different effective area features, the in-flight calibration programme has used a number of targets possessing simple power-law spectra, such as plerionic supernova remnants and AGN. Anomalous residual features in the fitted spectra are used to highlight discrepant features in the effective area (mainly confined to absorption edges) and response functions (mainly low energy residuals in absorbed sources). This work is still in progress, but already the calibration goals for allowing the first release of data to guest observers have been met, and exciting science is already enabled. We use the initial response matrices as a baseline for testing aspects of mode performance and blocking filter transmission as described in the rest of the paper.

4. MODE PERFORMANCE

One characteristic of CCD detectors that is in marked contrast with prompt (i.e. gas and M.C.P.) counters, is the finite readout time, which makes CCDs prone to pile-up effects: The energy resolving capability is compromised when two or more photons are detected in a pixel, or adjacent pixels, in one readout frame. Such degradation is minimised in EPIC by an appropriate choice of flexible readout modes. A reduced size window can be selected for the CCD at the focal point of each camera, reducing the frame time for readout, and the fraction of piled-up events in proportion.

Mode Name	Field of View (arc min)	Comment	Frame Time	Pt. Source Flux (mCrab)
PN			(ms)	
Full Frame	27.5 x 26.4	7% out of time events	73	1
Full Frame Extended	27.5 x 26.4	Reduced out of time events	200	0.3
Small Window	4.4 x 4.4	One CCD only	6	15
Large Window	13.8 x 26.4	A frame-store mode	45	2
Timing	4.4 x 13.8	1-d imaging only	0.03	150
Burst	4.4 x 1.4	Low duty cycle	0.007	6000
		For Timing and Burst modes Frame time = source integration *time*		
MOS			(s)	
Full Frame	33 x 33		2.6	0.5
Small Window	1.8 x 1.8	For inner CCD	0.3	15
		Outer CCDs full coverage	2.7	
Large Window	5.5 x 5.5	For inner CCD	0.9	4
		Outer CCDs full coverage	2.7	
Timing	1.8 x 10	1-d imaging	0.001	150
		Outer CCDs full coverage	2.7	

Table 2. Summary of EPIC readout modes used in flight

A trade-off has to be made in selecting such modes. A very small window does not encompass all the energy enclosed in the Point Spread Function (PSF), and flux loss outside the window must be accounted for, in determining the effective area. In slow readout modes, pile-up in the core of the PSF also leads to flux loss. In both cases the flux loss is energy dependent. Pile-up itself leads to the combining of multiple low energy photon signals into single events of higher energies. In other words piled-up spectra show spectral hardening and flux loss. These effects are discussed in reference 11. Guest Observers applying to use EPIC were advised that a count rate not exceeding 1 photon/CCD readout ensures minimal spectral distortion due to pile-up. Following initial commissioning tests, the performance of readout modes of the two camera types have been consolidated. Table 2 indicates their summary parameters, including flux rate capability based on the above criterion.

The MS0737+7441 AGN exhibits a simple absorbed power law spectrum, and was observed in two different modes in EPIC MOS. The extracted spectral fit parameters are shown in Table 3. This table shows that not only are measurements in different modes consistent, but also that the spectral distortion at a few counts/second is negligible.

An extreme example of count rate capability is provided by the observations of black-hole binary, LMC X-3. This was observed to provide a high S:N measurement in the PSF wings. The piled-up core was ignored (Figure 5), and spectra from outer regions were extracted in two exposures with different modes. Again the spectral fits are compared in the two modes (Table 4), and except for the normalisation factors (as expected due to pile-up flux losses), are very similar. This demonstrates that reliable spectral fitting can still be obtained by appropriate data selections on targets far brighter than nominal limits in Table 2.

MOS Mode	Counts/Frame	Hydrogen Column	Power Law	Normalisation
Full Frame	3.6	4.16 ±0.10	2.39±0.05	2.16±0.05
		(x 10^{20}cm^{-2})		(x 10^{-3})
Large Window	1.2	4.28±0.13	2.41±0.03	2.24±0.04

Table 3. Comparison of spectral fitting results in different EPIC readout modes

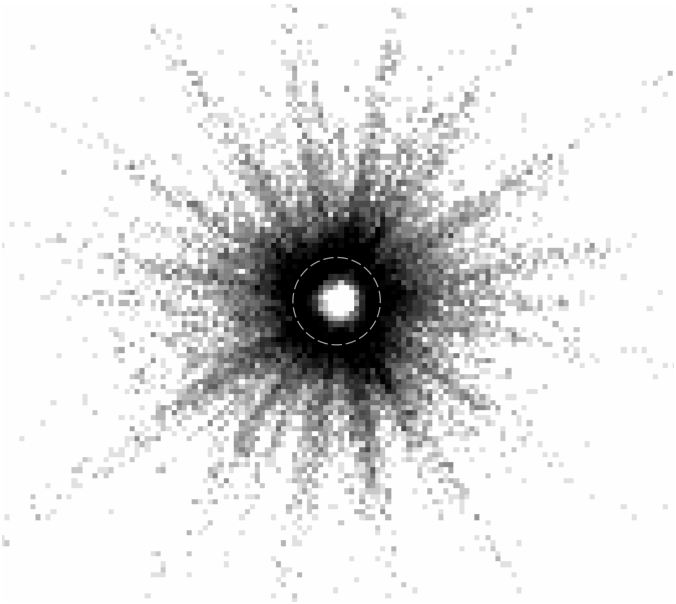

Figure 5. Zoomed and log-scaled image of LMC X-3 PSF (EPIC MOS). Dashed circle indicates limit of region of piled-up core to be excised (∼13 arcsecs radius)

MOS Mode	Cts/sec (Measured)	Cts/Frame (Inferred)	H Column (x 10^{20}cm^{-2})	Disc Temp (keV)	Norm.	Power Law	Norm. (x 10^{-2})
Full Frame	10.8	126	9.1 ±0.6	0.8±0.03	5.45±0.46	2.60±0.07	1.07±0.07
Large Window	11.3	44	9.0±0.43	0.75±0.02	7.34±0.47	2.57±0.04	1.15±0.05

Table 4. Results of spectral fitting achieved on LMCX-3 data, after excision of the pile-up core

A final note on the use of readout modes is that both EPIC cameras provide a timing capability through continual readout modes. In the PN case this is demonstrated with observations of X-ray pulsars, where the rapid readout allows $\ll$millisecond resolution or the ability to measure bright targets without imaging pile-up. Figure 6 shows the folded pulse profile of PSR0540-69, re-binned at 1msec samples.

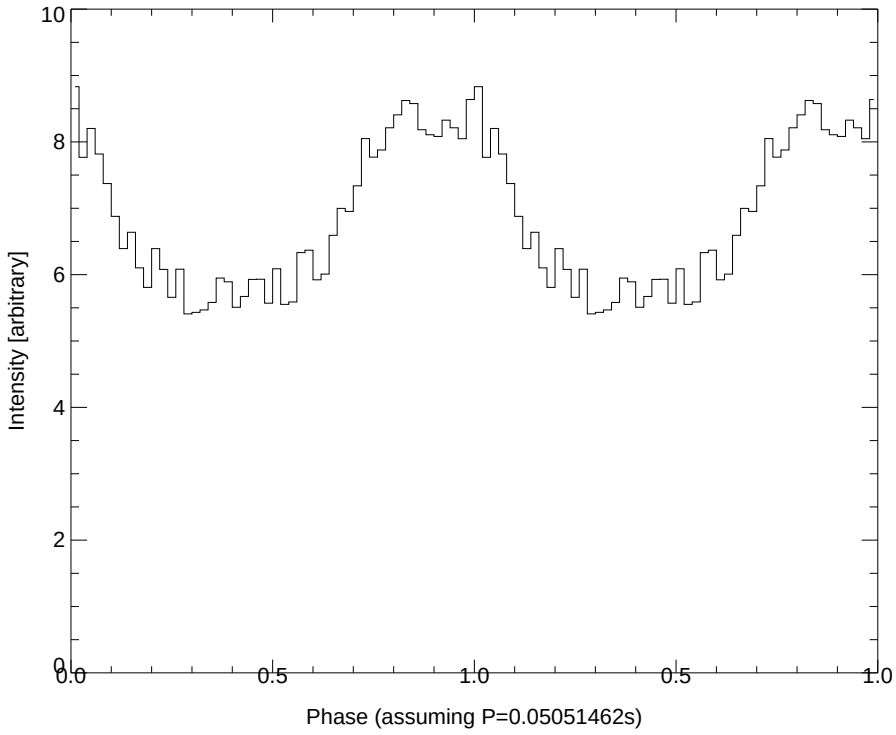

Figure 6. EPIC PN observation of PSR0540-69 in timing mode. Data rebinned and folded to 1msec time resolution

5. OPTICAL BLOCKING FILTERS

Visible photons produce a signal in the X-ray cameras indistinguishable from that of X-ray photons. This additional background signal creates an offset in the X-ray energy scale and an additional shot noise component. This noise degrades the energy resolution and contributes to a change in response distribution function. The filter wheel in EPIC carries different optical blocking filters optimised for particular investigations. The thick filter comprising 200nm Al on a 350nm polypropylene support, reduces optical flux below 1 electron per pixel per frame for stars as bright as 0 magnitude. Medium and thin filters produced with 80 or 40 nm of Al on 160nm polyimide films have a higher transmission for soft X-rays, but with magnitude limits for minimal noise degradation of $\sim$8 and 14 respectively.

Their performance is verified with observations of the CAL83 super-soft source. In Figure 7 we show the results of spectral fitting of a black body spectrum with interstellar photoelectric absorption and an broad absorption edge representing the NLTE absorption models. In this case the observation was made with the THIN filter. In Figure 8 this fixed model is compared with response in the MEDIUM and THICK filters. This illustrates the significant improvement in soft X-ray response that can be achieved by an appropriate choice of filter. If EPIC had been deployed with a fixed filter, with an aluminium thickness necessary to attenuate optical light from most stellar targets, a significant factor $\sim$3 reduction in soft X-ray collection area would have been suffered, compared with the thinnest of filters now employed. With its set of filters, EPIC can now provide an energy response over two decades, from 0.15 to 15keV.

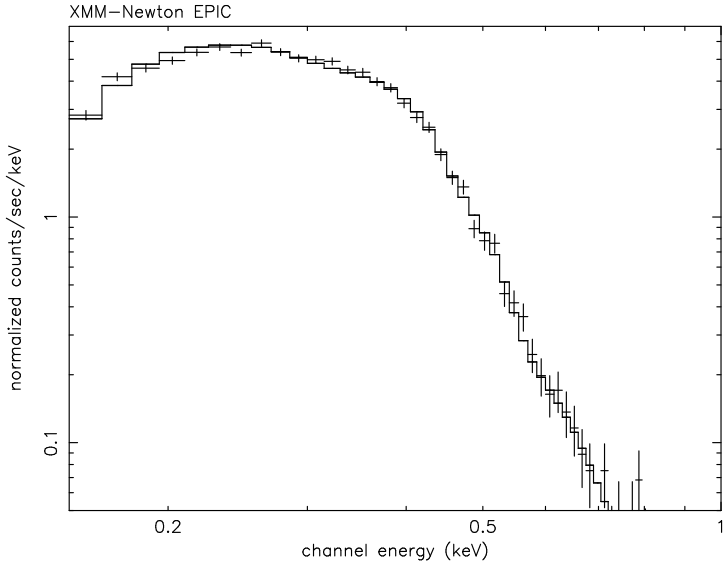

Figure 7. Data and model fit for CAL83 source in EPIC MOS THIN filter

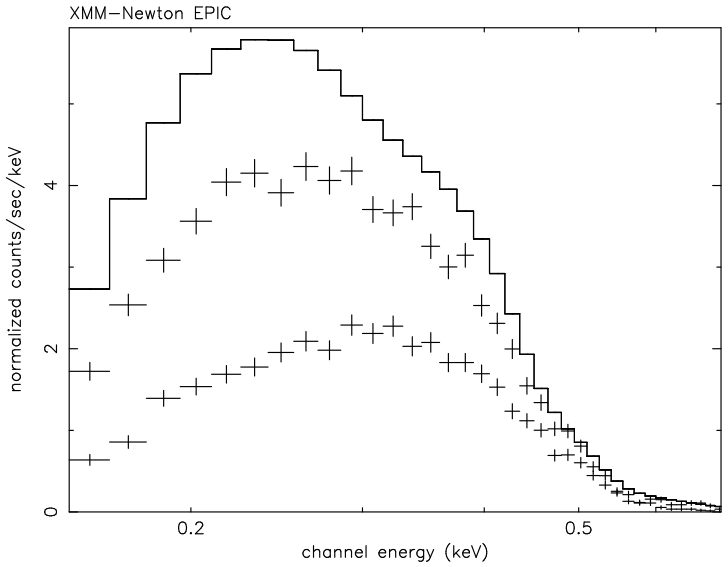

Figure 8. Comparison of THIN filter response (upper histogram) to CAL83 super soft source, with data points measured with MEDIUM (middle) and THICK (lower) filters

6. CONCLUSIONS

The photon energy determinations have not been significantly degraded since launch, and the effective area of the EPIC cameras seems to meet all expectations. The calibration knowledge, following modifications deduced as a result of a comprehensive in-flight calibration programme, is already acceptable to start performing scientific investigations of the Guest Observer programme. The final refinements for energy response will be challenging to achieve, and need to consider details of mode pile-up performance and optical light leakage. Nevertheless we demonstrate that the basic expectations of count rate capability and filter transmissions are amply confirmed

ACKNOWLEDGMENTS

We are grateful to our colleagues from the XMM−Newton Science Operation Center, at Villafranca Satellite Tracking Station, Madrid, Spain. Their support in implementing the in-orbit calibration programme in many diverse operational aspects was invaluable. Many thanks also go to the development team of the XMM−Newton Science Analysis Software, which was used for much of this work. The data shown in Figure 4 were provided from Guranteed Time Observations of Prof. J. Bleeker, of the Space Research Organisation Netherlands. We gratefully acknowledge the use of this data to help to demonstrate the capabilities of the EPIC cameras.

7. REFERENCES

1 F. Jansen, "XMM: Advancing Science with the High-Throughput X-ray Spectroscopic Mission", ESA bulletin 100, pp.15-20, 1999.
2 Ph. Gondoin, D. de Chambure, K. van Katwijk, Ph. Kletzkine, D. Stramacicioni, B. Aschenbach, O. Citterio, R. Willingale, "The XMM Telescope", SPIE Proc.2279, pp.86-100, 1994.
3 A.D.Holland, M.J.L.Turner, A.F.Abbey, P.J. Pool, "MOS CCDs for the EPIC on XMM", SPIE Proc.2808, pp. 414-420, 1996.
4 N. Meidinger, H.W. Brauninger, R. Hartmann, G. Hartner, N. Krause, E. Pfeffermann, C. Reppin, G. Schwaab, L. Struder, J. Trumper, P. Holl, J. Kemmer, S. Krisch, H. Soltau, C. van Zanthier, D. Hauf, R. Richter, "PN-CCD detector for the European Photon Imaging Camera on XMM", SPIE Proc.2808, pp. 492-503, 1996.
5 A.C.Brinkman, H.J.M.Aaarts, A.J.F.den Boggende, L.Dubbeldam, J.W.den Herder, J.S.Kaastra, P.A.J.de Korte, R.Mewe, C.J.Hailey, S.M.Kahn, F.B.S.Paerels, G.Branduardi-Raymont, J.V.Bixler, K.Thomsen, A.Zehnder, "Reflection Grating Spectrometer on-board XMM", SPIE Proc.2808, pp. 463-480, 1996.
6 R. Much, D. Lumb, M.S. Cropper, R. Hunt, K.O. Mason, F.A. Cordova, T. Sasseen, C. Ho, W. Priedhorsky, C.Jamar, E. Antonello, "The Optival/UV Monitor on the X-ray Multi Mirror Mission",Proceedings of the Conference " Ultraviolet Astrophysics, Beyond the IUE Final Archive", Sevilla, Spain, ESA SP-413, p.815, 1998.
7 M.J.L. Turner et al, Presented at SPIE 4012
8 U.G.Briel , Proceedings SPIE 4012, in press 2000
9 Ph. Gondoin et al, these Proceedings
10 L.K. Townsley, P. Broos, G. Garmire, J. A. Nousek, "Mitigating Charge Transfer Inefficiency in the Chandra X-Ray Observatory Advanced CCD Imaging Spectrometer", Astrophysical Journal 534, L139-L142, 2000
11 J. Ballet, "Pile-up on X-ray CCD instruments", Astronomy and Astrophysics Supplement 135, p.371-381, 1999
12 P. Marty, et al, These Proceedings
13 C. Pigot C., J.L. Sauvageot, P. Ferrando and E.Belsole, these proceedings